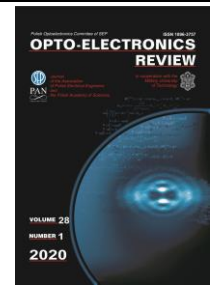


# Effat University Repository

## A complexity efficient PAPR reduction scheme for FBMC-based VLC systems

Authors	Radwa A Roshdy;Hussein, Aziza;Mohamed M Mabrook;Mohammed A Salem
DOI	<a href="https://doi.org/10.24425/opelre.2023.144919">https://doi.org/10.24425/opelre.2023.144919</a>
Publisher	Polish Academy of Sciences and Association of Polish Electrical Engineers in cooperation with Military University of Technology
Download date	2026-04-22 06:03:42
Link to Item	<a href="http://hdl.handle.net/20.500.14131/891">http://hdl.handle.net/20.500.14131/891</a>



# A complexity efficient PAPR reduction scheme for FBMC-based VLC systems

Radwa A. Roshdy<sup>1</sup>, Aziza I. Hussein<sup>2</sup>, Mohamed M. Mabrook<sup>3,4</sup>, Mohammed A. Salem<sup>1\*</sup>

<sup>1</sup>Department of Electrical Engineering, Higher Technological Institute, 10th of Ramadan City, Egypt

<sup>2</sup>Electrical & Computer Eng. Dept., Effat University, Jeddah, Saudi Arabia

<sup>3</sup>Space Communication Dept., Faculty of Navigation Science & Space Technology, Beni-Suef University, Beni-Suef, Egypt

<sup>4</sup>Department of Communication and Computer Engineering, Faculty of Engineering, Nahda University in Beni-Suef, Egypt

## Article info

### Article history:

Received 18 Nov. 2022

Received in revised form 23 Jan. 2023

Accepted 02 Feb. 2023

Available on-line 27 Mar. 2023

### Keywords:

Visible light communication; filter bank multicarrier; peak-to-average power ratio reduction; computational complexity; cube satellite communication link; inter-satellite communications.

## Abstract

Visible light communication based on a filter bank multicarrier holds enormous promise for optical wireless communication systems, due to its high-speed and unlicensed spectrum. Moreover, visible light communication techniques greatly impact communication links for small satellites like cube satellites, and pico/nano satellites, in addition to inter-satellite communications between different satellite types in different orbits. However, the transmitted visible signal via the filter bank multicarrier has a high amount of peak-to-average power ratio, which results in severe distortion for a light emitting diode output. In this work, a scheme for enhancing the peak-to-average power ratio reduction amount is proposed. First, an algorithm based on generating two candidates signals with different peak-to-average power ratio is suggested. The signal with the lowest ratio is selected and transmitted. Second, an alternate direct current-biased approach, which is referred to as the addition reversed method, is put forth to transform transmitted signal bipolar values into actual unipolar ones. The performance is assessed through a cumulative distribution function of peak-to-average power ratio, bit error rate, power spectral density, and computational complexity. The simulation results show that, compared to other schemes in literature, the proposed scheme attains a great peak-to-average power ratio reduction and improves the bit the error rate performance with minimum complexity overhead. The proposed approach achieved about 5 dB reduction amount compared to companding technique, 5.5 dB compared to discrete cosine transform precoding, and 8 dB compared to conventional direct current bias of an optical filter bank multicarrier. Thus, the proposed scheme reduces the complexity overhead by 15.7% and 55.55% over discrete cosine transform and companding techniques, respectively.

## 1. Introduction

Visible light communication (VLC) is a communication system where data is sent after it is modulated using visible light waves. In general, any system where data is sent using any visible light to human eyes can be called VLC [1–3]. Nevertheless, this type of communication was based on transmitting information in a manner that is invisible to human vision, so that all that could be seen is

the normal ambient illumination without any noticeable difference [1]. VLC is considered as a viable solution for the increasing demand of high capacity and ubiquitous connectivity in the next standard wireless networks (e.g., 5G, satellite and beyond), as the radio frequency (RF) spectrum becomes congested and overused [4–6]. VLC has a large unlicensed spectrum with the range from 400 THz to 700 THz which is ten thousand larger than the entire RF spectrum [7, 8]. It also provides low latency data transmission compared to RF transmission, due to its high speed. Moreover, VLC is more immune to interference, which

\*Corresponding author at: [mohammed.adel@hti.edu.eg](mailto:mohammed.adel@hti.edu.eg)

makes it widely used in indoor environments such as hospitals, aircrafts, etc. [9, 10]. Light emitting diode (LED) technologies, have become more prominent and accessible, providing new contexts for VLC technology [11]. Also, using a laser diode (LD) instead of LED has gained more attention due to its increase in modulation bandwidth (approximately 1 GHz), efficient optical power, convergence of the light beam, and simultaneous illumination [12].

Filter bank multi carrier (FBMC) communication is a promising waveform design candidate in incoming intensity modulation/direct detection (IM/DD)-based VLC system by RF/VLC networks [13–15]. This is due to several reasons: i) it has lower out-of-band (OOB) emissions [16]; ii) it has higher spectrum efficiency because it does not use cyclic prefix (CP) [17]; iii) it has higher immunity to environment effects such as scattering and shadowing [18]. Even though VLC-FBMC systems and RF-FBMC both have significant peak-to-average power ratio (PAPR), VLC-FBMC systems cannot be directly reduced using conventional PAPR reduction techniques [19], due to some differences between both systems. First, the transmitted RF-FBMC waveform is complex-valued [20], whereas the VLC-FBMC waveform is real-valued [21]. As a result, the lower and upper PAPRs of a real-valued FBMC waveform must be decreased. Second, in RF transmission, both in-band distortions and out-of-band power loss are compensable using PAPR enhancement techniques [20]. Nevertheless, as LED can be considered a low-pass filter in visible FBM systems, out-of-band subcarriers cannot be used to send symbols [21]. Consequently, OOB interferences are not considered, which provides a flexible PAPR reduction method for VLC-FBMC systems [22]. Moreover, high PAPR requires considerable biasing to convert the bipolar FBMC waveform to unipolar, causing the system to be optically inefficient [23]. As a result, PAPR decreasing becomes a necessary part of a VLC-FBMC.

The reduction of bit error rate (BER) and computational error rate, in addition to the enhancement of power spectral density (PSD), beside efficient complexity-based PAPR reduction scheme, results in evolving new communication technologies, especially satellite communication.

There are two main promising space technologies based on VLC according to free-space optical communications for Space FOCS project [2]. The first application scenario deals with transmitting Gbit/s signals on small satellites, e.g., CubeSats and MicroSats. The second selected research line is a low-bit-rate communication between satellites, e.g., inter-satellite communications [2, 6, 12].

VLC-FBMC PAPR reduction techniques are divided into four categories: signalling scrambling technique, coding technique, pre-distorting signal technique, and spreading technique [24]. In the signalling and scrambling technique, there are partial transmit sequences (PTS) and selective mapping (SLM), in which a step rotation factor value is adjusted, and a signal with the lowest PAPR is chosen for transmission [25]. However, this is achieved at the expense of many side information bits, reducing spectral efficiency and increased computational complexity overhead [26]. The clipping technique is the most common example of a pre-distorting signal technique, in which a signal amplitude that is larger than a pre-determined value is clipped, resulting in a reduction in PAPR. Nevertheless, the performance of BER becomes the worst [27]. Although

spreading PAPR reduction techniques [i.e., discrete Fourier transform (DFT) spreading, Hadamard spreading] have lower complexity overhead and improve the performance of BER, the PAPR reduction amount is marginal [28]. In the literature review, several techniques were proposed to reduce PAPR for RF-FBMC. However, there were few prior works that concerned reducing PAPR in FBMC-based VLC systems. A hybrid technique between the categories was proposed in several works. In Ref. 29, a combination of a discrete cosine transform (DCT), and a spreading and clipping method was introduced to enhance the PAPR reduction amount. In Ref. 30, PAPR was reduced through three layers based on the clipping method. In Ref. 31, a modified overlapped selective mapping (M-OSLM) suppression technique was proposed to enhance the PAPR reduction amount.

In contrast, the methods which provide lower complexity overhead have a quite notable PAPR reduction over using the conventional PAPR reduction techniques. Motivated by the previous issues, in this paper, a new technique for the FBMC-based VLC system is proposed, whose waveform PAPR is inherently reduced with a negligible SI and without any increase in complexity overhead. The major contributions are summarised as follows:

1. A new PAPR reduction scheme is proposed through two steps:
  - a. First, two candidate waveforms are generated by using the circular time-shift property of the inverse discrete Fourier transform (IDFT). The waveform with the lowest PAPR is chosen to be transmitted. This is achieved with lower complexity overhead compared to a conventional DC-bias optical FBMC (DCO-FBMC) system.
  - b. Second, an alternative method to DC bias is proposed to satisfy purely real positive values for a transmitted waveform. The alternative method is based on separating positive and negative values in the transmitted signal. Then, the negative values were added together by the number of cascaded adders and, finally, reversed before concatenating with the positive part.
2. The performance evaluation of the proposed technique is presented through PAPR complementary cumulative distribution function (CCDF), BER, complexity overhead, and PSD at different numbers of subcarriers.
3. The simulation results show that the proposed scheme attains an extra amount of PAPR reduction with lower BER and complexity overhead compared to other relevant PAPR reduction techniques in the literature.

The rest of the paper is organised as follows: in section 2, the conventional FBMC-based VLC is reviewed. The proposed PAPR reduction scheme is introduced in section 3. In section 4, the performance of the proposed scheme is investigated with respect to other literature schemes. Finally, the paper conclusions are introduced in section 5.

## 2. FBMC-based VLC conventional system

Figure 1 shows the structure of FBMC-based VLC transceiver. Denoting the number of subcarriers by  $N$ , number of symbols in each subcarrier is  $N$ . As shown in Fig. 1, the  $m^{\text{th}}$  complex symbol at  $n^{\text{th}}$  subcarrier is applied

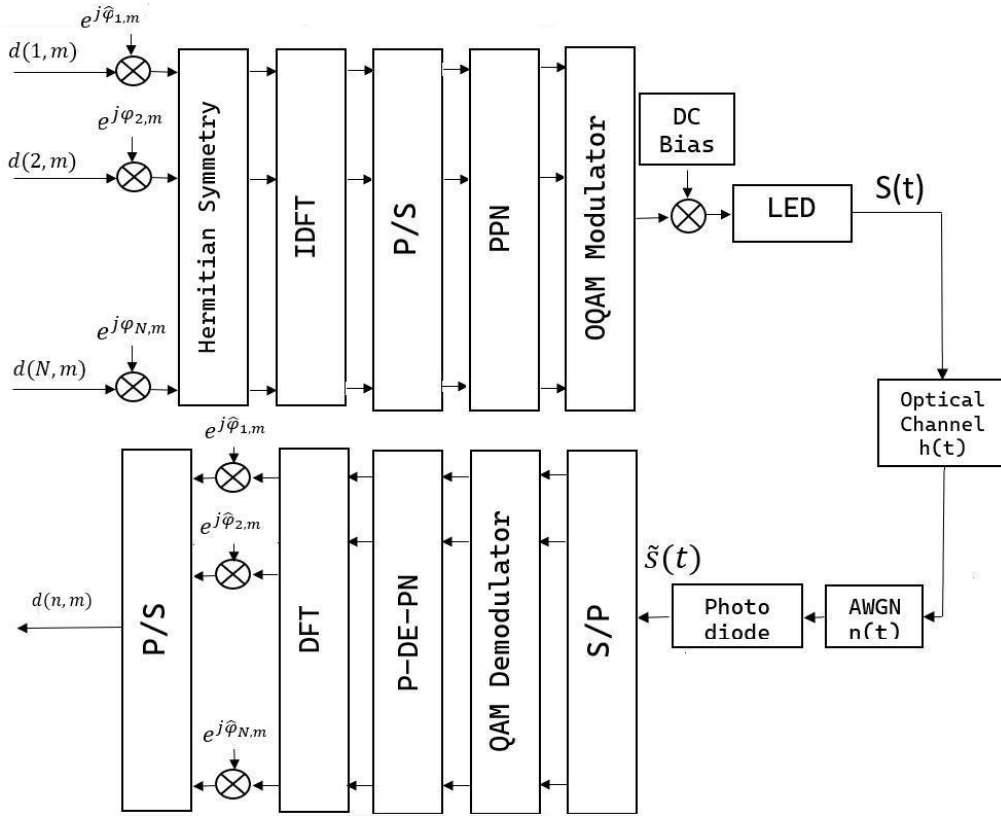


Fig. 1. The FBMC-based VLC transceiver.

to the FBMC input at the transmitter. The complex input data symbol is first multiplied to the phase shift pattern  $e^{j\varphi_{n,m}}$  where  $\varphi_{m,n} = \varphi_o + \frac{\pi}{2}(m+n) \bmod \pi$ . The purpose of using a phase shift is to make a  $\pi/2$  phase shift between the neighbouring symbols transmitted along time and frequency [20].

Hermitian symmetry (HS) before IFFT is used for the purpose of providing a real output, by using a double number of IFFT/FFT points at transmitter and receiver [32]. Each subcarrier is individually filtered using what is called a prototype filter, which is a real symmetric filter. The ratio between duration of a filter impulse response and duration of a symbol on each subcarrier is defined by the overlapping factor  $k$ , and it is the main characterisation of the prototype filter. The value of  $k$  determines how inter-symbol interference (ISI) is suppressed. At  $k = 4$ , the ISI is significantly removed [33].

The individually filtered subcarrier is achieved with no need of frequency spreading, by utilizing a poly phase network (PPN) where the output vector of IFFT is copied  $K$  times and is multiplied to the prototype filter  $h(t)$ . Finally, a quadrature amplitude modulation (QAM) offset is used to introduce a  $T/2$  time offset between the in-phase and quadrature phase component of the PPN output to guarantee orthogonality between adjacent subcarriers [34]. The transmitted waveform via FBMC is in a complex form, and this is not acceptable in VLC system, as the transmitted visible signal must be real and positive. Consequently, the DC bias is widely used in the conventional VLC system at the end of the transmitter [13]. The continuous time domain for the FBMC VLC waveform according to the implementation shown in Fig. 1 is given by

$$s(t) = \sum_{N=0}^{N-1} \sum_{m=0}^{M-1} d(n,m) f(t - mT) e^{j\frac{2\pi n t}{T}} e^{j\varphi_{n,m}}, \quad (1)$$

where  $d(n,m)$  is the  $m^{\text{th}}$  complex FBMC input symbol,  $T$  is the duration of complex input symbol  $d(n,m)$  for each subcarrier,  $f(t - mT)$  is the prototype filter with a length of  $KN$  denoted by  $L$ , and  $M$  is the number of offset-quadrature amplitude modulation (OQAM) symbols per each subcarrier.

The impulse response of the prototype filter in time domain is given by

$$f(t) = 1 + 2 \sum_{k=1}^K (-1)^k G_k \cos\left(2\pi \frac{kn}{L}\right), \quad (2)$$

where  $H_k$  is the set of the filter coefficients at overlapping factor  $K$  which is defined as follows:

$$\begin{aligned} G(0) &= 1 \\ G\left(\frac{1}{L}\right) &= 0.97169 \\ G\left(\frac{2}{L}\right) &= \frac{1}{\sqrt{2}} \\ G\left(\frac{3}{L}\right) &= 0.235147 \\ G\left(\frac{i}{L}\right) &= 0.4 \leq i \leq L-1. \end{aligned} \quad (3)$$

The unipolar positive signal is transmitted through the optical channel  $h(t)$  to the analysis filter bank (AFB) at the

receiver. It is first detected by using a photodiode (PD) before applying a QAM modulator, poly diphase network (PDE-PN), and DFT to recover the original complex data symbols. This is represented as follows

$$\tilde{s}(t) = R s(t) \otimes h_{los}(t) + n(t), \quad (4)$$

where  $\tilde{s}(t)$  is the received signal,  $R$  is the PD responsivity,  $s(t)$  is the transmitted signal,  $h_{los}(t)$  is the line of sight (LoS) optical channel impulse response and  $n(t)$  is the additive white Gaussian noise (AWGN) with zero mean and the summed variance  $\sigma^2$  of thermal noise and shot noise.

### 3. The proposed PAPR reduction scheme

#### 3.1. Proposed DCO-FBMC algorithm

It is obvious from Fig. 1 that the input complex symbols are multicarrier modulated with IDFT, before applying the OQAM concept. If the IDFT cyclic time-shift property is applied to the IDFT output vector, the multicarrier modulation is also obtained. The output IDFT signal is denoted by  $D(n, m)$ , which is given by

$$D(n, m) = \sum_{n=0}^{N-1} d(n, m) e^{j\left(\frac{2\pi}{N}\right)n}. \quad (5)$$

Denoting the IDFT cyclic time-shift by  $X(n, m)$  is given by

$$X(n, m) = \left[ \mathbf{D}\left(\frac{N}{2}:N\right) \mathbf{D}\left(0:\frac{N}{2}\right) \right]. \quad (6)$$

From (5) and (6), it is obvious that the PAPR of transmitted signals depends on IDFT and DFT, with a cyclic time-shift property that is nearly the same because the DFT cyclic time-shift property swaps the left and the right half parts of the IDFT output vector. However, after applying the PPN, both IDFT output and IDFT circular time-shift output have different PAPR. This is because the in-phase channel symbols which overlap with the quadrature channel symbols are different in IDFT  $D(n, m)$  and circular time-shift IDFT  $X(n, m)$  versions. As a result, the parts of the candidate waveform outside the overlapped interval, depending on which symbols of two versions of waveform are overlapped, are not the same. Thus, the PAPRs of the two signals differ from one another. The PAPR of the two versions,  $D(n, m)$  and  $X(n, m)$  are compared and the version with the lowest peak power is picked and transmitted. Consequently, the symbols with minimum PAPR will be transmitted and the symbols with higher PAPR will be rejected. As shown in Fig. 2, switch (SW) is used after IDFT, with one bit control. When SW = 0, this means that the IDFT candidate signal is generated, and the visible transmitted signal is denoted by  $s^1(t)$ . If SW = 1, the cyclic time-shift DFT signal is generated, and the visible transmitted signal is denoted by  $s^2(t)$ . The PAPR of the two signals is calculated for each symbol, and the symbol with the lowest PAPR is chosen and concatenated with the next symbol chosen to achieve the lowest PAPR.

Let us assume that  $C(t)$  denotes the concatenated signals. It is produced as follows

$$C(t) = s_{bipolar}^{(r)}(t), \quad (7)$$

where  $(r)$  is the index of the selected candidate symbol. For the first block ( $m = 0$ ), it is calculated as follows

$$r = \operatorname{argmin}_{a \in \{1,2\}} \left\{ \max |s_{bipolar}^a(t)|^2 \right\}. \quad (8)$$

For ( $m \geq 1$ ), the peak power is calculated by

$$C(t) = C_{m-1}(t) + s_m^{(r)}(t) \quad (9)$$

and not  $s^a(t)$  because  $C_{m-1}(t)$  and  $s_m^{(a)}(t)$  overlap due to pulse shaping and OQAM IQ staggering. The index of the selected candidate signal is defined as follows:

$$r_m = \operatorname{argmin}_{a \in \{1,2\}} \left\{ \max |C_{m-1}(t) + s_m^{(a)}(t)|^2 \right\}. \quad (10)$$

At the end of the symbols, the chosen signal is with a low PAPR and is transmitted after it is applied to DC bias, as shown in Fig. 2.

At the receiver, the PD is used to detect the optical unipolar signal. Every symbol in the received signal is determined, depending on whether it is IDFT candidate or DFT cyclic time-shift, according to the appended control bit at the beginning of the symbol block. If the control bit is zero, this means that the received signal belongs to the IDFT vector output and the SW at the receiver will be turned off. If the control bit is one, this implies that the received signal belongs to DFT cyclic time-shift vector output and the SW will be turned on. This can be given as follows:

$$\tilde{s}(t) = \begin{cases} s^1(t) & \text{if control bit} = 0 \\ s^2(t) & \text{if control bit} = 1. \end{cases} \quad (11)$$

#### 3.2. Addition reversed FBMC

Thanks to its higher spectral efficiency, DCO-FBMC is widely used in the FBMC-based VLC system. However, higher consuming energy is a clear challenge when obtaining a positive unipolar signal from a real bipolar one [35]. As a result, it is essential to replace DC bias with another fast and efficient approach that involves minimum losses in spectral efficiency and energy consuming. In this context, the authors suggest a different approach to DC bias which they call the addition reversed FBMC. As shown in Fig. 3, the authors divided the transmitted bipolar real VLC-FBMC signal into a positive and negative unipolar signal which is given by

$$s(t)_{bipolar} = s(t)_{unipolar}^+ + s(t)_{unipolar}^- \quad (12)$$

The positions of positive and negative values in  $s(t)_{unipolar}^-$  and  $s(t)_{unipolar}^+$ , respectively, have zero power to prevent interference and obtain accurate detection at the receiver. This can be expressed as follows:

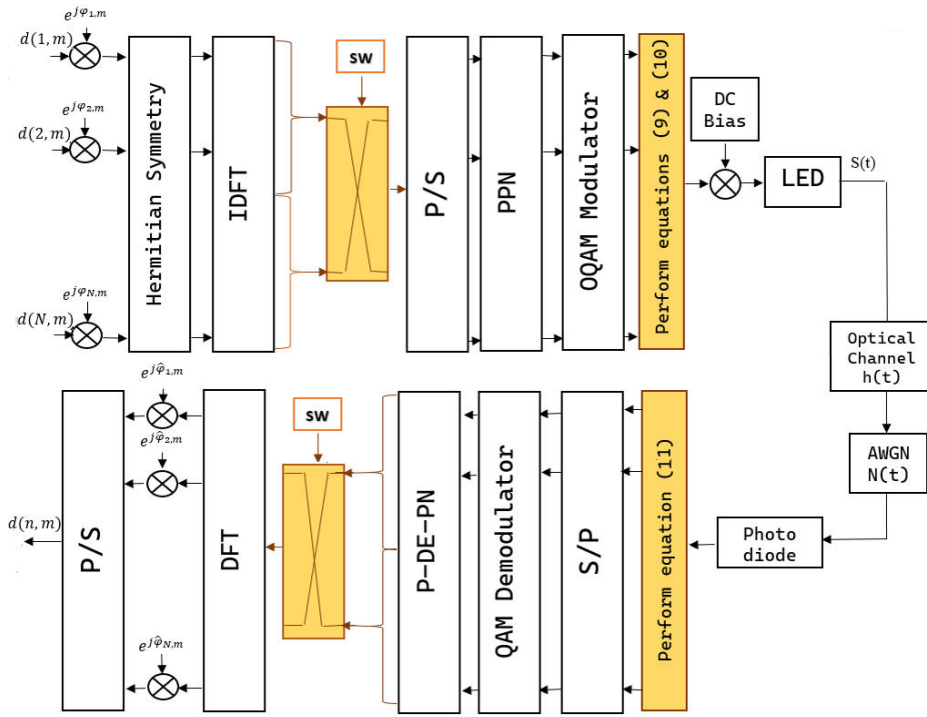


Fig. 2. The transceiver structure of FBMC VLC-based proposed candidate algorithm.

$$s(t)_{\text{unipolar}}^+ = \begin{cases} s(t)_{\text{unipolar}}^+ & s(t)_{\text{bipolar}} > 0 \\ 0 & \text{otherwise} \end{cases} \quad (13)$$

$$s(t)_{\text{unipolar}}^- = \begin{cases} s(t)_{\text{unipolar}}^- & s(t)_{\text{bipolar}} < 0 \\ 0 & \text{otherwise} \end{cases} \quad (14)$$

The negative unipolar signal is added up with itself, and the output of this summation is in turn added up with the original unipolar negative. In other words, the unipolar negative signal is applied to a consecutive number of adders and the output of each adder is applied to a next one, as shown in Fig. 3.

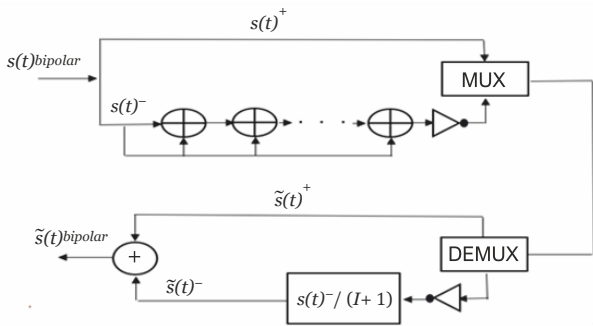


Fig. 3. The added reversed FBMC structure.

Then, the final summation output is reversed and multiplexed to the positive unipolar waveform, so that the transmitted visible signal is defined by

$$s(t) = s(t)_{\text{unipolar}}^+ + (I + 1)s(t)_{\text{unipolar}}^-, \quad (15)$$

where  $I$  is the number of consecutive adders. Using the addition rule to the negative signal helps to reduce PAPR. However, the PAPR is still high. Using the addition rule to the negative signal helps to reduce PAPR.

When the visible FBMC signal is sent to the receiver, it must be compatible with IM/DD to be detected into an electrical signal. After that, the electrical signal is demultiplexed into two parts, as follows:

$$\tilde{s}(t) = \begin{cases} \tilde{s}(t)_{\text{unipolar}}^+ & 0 \leq m \leq \frac{M}{2} \\ (I + 1)\tilde{s}(t)_{\text{unipolar}}^- & \frac{M}{2} + 1 \leq m \leq M \end{cases} \quad (16)$$

**Algorithm 1:** FBMC-based VLC PAPR reduction scheme.

- 1 **Input:** number of subcarriers  $N$ , number of symbols  $M$
- 2 **While**  $m > M$  **do**
- 3 **For**  $n = 1 : N$
- 4 Calculate the first candidate IDFT signal  $s_m^1(t)$
- 5 Calculate the first candidate cyclic time-shift DFT signal  $s_m^2(t)$
- 6 Apply  $s_m^1(t)$  to the addition reversed FBMC
- 7 Apply  $s_m^2(t)$  to the addition reversed FBMC
- 8 Calculate  $\text{PAPR}_1(n)$  for the addition reversed FBMC output when input is  $s_m^1(t)$
- 9 Calculate  $\text{PAPR}_2(n)$  for the addition reversed FBMC output when input is  $s_m^2(t)$
- 10 **If**  $\text{PAPR}_1(n) > \text{PAPR}_2(n)$
- 11  $s_m^1(t)$  is selected
- 12 **else**
- 13  $s_m^2(t)$  is selected
- 14 **end**
- 15 Calculate (18)
- 16 **end**
- 17 **end**

Then, the negative unipolar part is obtained by dividing it by  $(I+1)$ , and then inverting its polarity. The positive and negative unipolar parts are then added to each other without interference because of using nulls of the reversed positions in each part individually.

For the improved BER performance, the candidate algorithm 1 is used after the reversed addition technique. This means that the proposed candidate algorithm is a positive unipolar signal. Therefore, equations (9) and (10) are updated to be:

$$r = \underset{a \in \{1,2\}}{\operatorname{argmin}} \{ \max |s_{bipolar}^a(t)|^2 \} \quad (17)$$

$$C(t) = C_{m-1}(t) + s_{bipolar, m}^{(a)}(t). \quad (18)$$

When the amplitude of the received signal is zero, the phase can be restored by using an algorithm such as the maximum likelihood algorithm. However, the addition reversed FBMC helps to reduce zero points of singularity and, as a result, BER performance is improved. The algorithm that indicates the overall proposed PAPR reduction scheme is illustrated in algorithm 1. Figure 4 shows the implementation of the proposed visible FBMC structure.

#### 4. Simulation results

In this section, the performance of the suggested scheme is evaluated in terms of PAPR and BER, with different number of multicarriers, compared to other PAPR reduction techniques in literature, namely DCT precoding [24] and A-law companding techniques. Moreover, a conventional DCO-FBMC was included in the comparison [36]. In the simulation, the visible light is sent from the

transmitter to the receiver through the LoS optical channel, which is defined by

$$h_{LoS}(t) = \frac{(m + 1)A_r}{2\pi d^2} \cos^m(\phi) \cos(\psi), \quad (19)$$

where  $A_r$  is the PD area detection,  $\phi$  and  $\psi$  are the light radiance angle of LED, and the light incidence angle of PD, respectively,  $d$  is the distance between LED and PD, and  $m$  is the Lambertian emission order given by

$$m = \frac{-\ln(2)}{\ln(\cos(\phi_{0.5}))} \quad (20)$$

where  $\phi_{0.5}$  is the half power of semi angle of LED.

Simulation results are validated through using a MATLAB software package. The simulation parameters and optical system parameters used in the simulation are given in Table 1. In simulation, the PAPR for each symbol of the optical FBMC system is calculated and is given as follows:

$$\text{PAPR} = \frac{\max_{(M) T \leq t \leq mT} |s(t)|^2}{E[|s(t)|^2]} \quad m = 1, \dots, M, \quad (19)$$

where  $E[|s(t)|^2]$  is the expected value of the visible FBMC transmitted symbols.

The PAPR performance is calculated by the CCDF as it is more widely used in PAPR reduction performance evaluation. CCDF is defined as the probability that PAPR goes beyond a given threshold value that is given by  $(\text{PAPR}_0)$ , where its smaller values represent better performance [20].

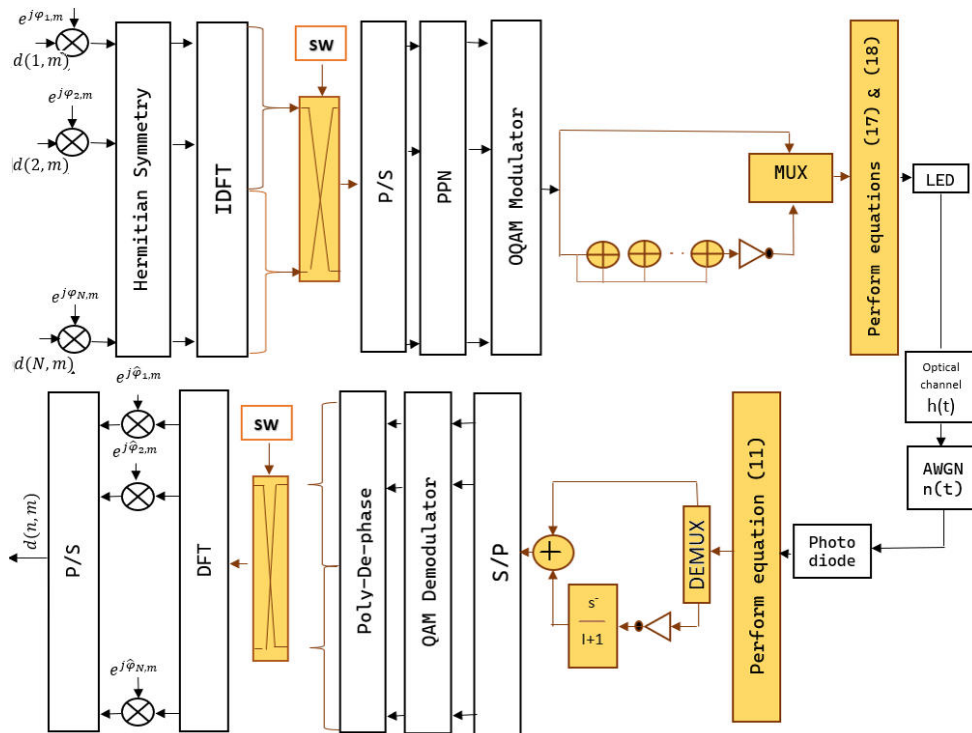


Fig. 4. The proposed visible FBMC structure.

**Table 1.**  
Simulation parameters.

Parameter	Value
FFT/IFFT size of FBMC	64, 128
Numbers of subcarriers ( $N$ )	64, 128
Numbers of symbols/subcarriers	$10^3$
DC bias	10 dB
PD responsivity	1
Energy bit to noise ratio ( $E_b/N_0$ )	10 dB
Channel models	Indoor VLC channel model with AWGN
Modulation	OQPSK*
Type of prototype filter	PHYDAYS filter
Overlap factor	4
half power of semi angle of LED ( $\phi_{0.5}$ )	$60^\circ$
light radiance angle of LED ( $\phi$ )	$40^\circ$
light incidence angle of PD ( $\psi$ )	$40^\circ$
PD area detection ( $A_r$ )	$1 \text{ cm}^2$
Distance between LED and PD ( $d$ )	2 m
PD responsivity ( $R$ )	1

\*Off-set quadrature phase shift keying.

Figure 5 illustrates the PAPR size of decrease for the proposed candidate algorithm with 64 and 128 subcarriers. This algorithm provides a further reduction in PAPR over the conventional DCO-FBMC. However, this reduction is limited to 1 dB~1.5 dB. This is due to the use of DC bias which results in the PAPR performance of the suggested algorithm. That is why the additional reversed FBMC as an alternative method to DC bias is proposed.

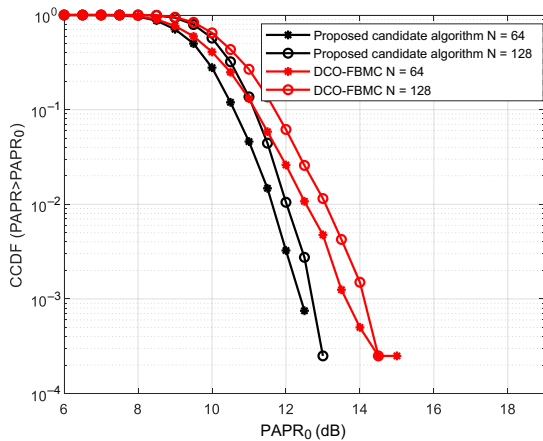


Fig. 5. PAPR CCDF of the proposed candidate algorithm.

As shown in Fig. 6, using the proposed algorithm in FBMC-based VLC systems influences the BER performance when the number of subcarriers from 64 and 128 is considered. When  $E_b/N_0 = 5 \text{ dB}$ , the proposed algorithm achieves  $\text{BER} = 10^{-3}$  while BER of DCO-FBMC is much lower than  $10^{-3}$ . This is because one bit of side information is added, by using a switch in the transmitter and receiver to each symbol of the candidate signals.

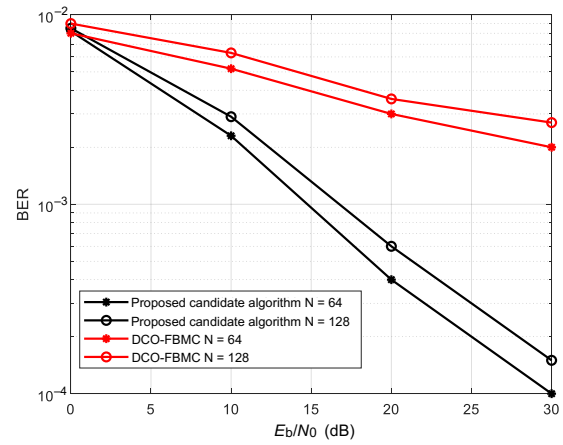


Fig. 6. BER performance of the proposed candidate algorithm.

Figures 7 and 8 show the PAPR CCDF of the proposed scheme with the subcarrier number  $N = 64$  and 128, respectively. Previous techniques such as DCT precoding and companding are included beside the conventional DCO-FBMC for the comparison. Figures 7 and 8 show that the suggested approach reduces PAPR by a significant amount. For instance, at  $\text{CCDF} = 10^{-3}$ , the proposed approach achieved about 5 dB reduction compared to the companding technique, 5.5 dB compared to the DCT precoding, and 8 dB compared to the conventional DCO-FBMC. The performance reduction of the suggested scheme is consistent with the number of subcarriers.

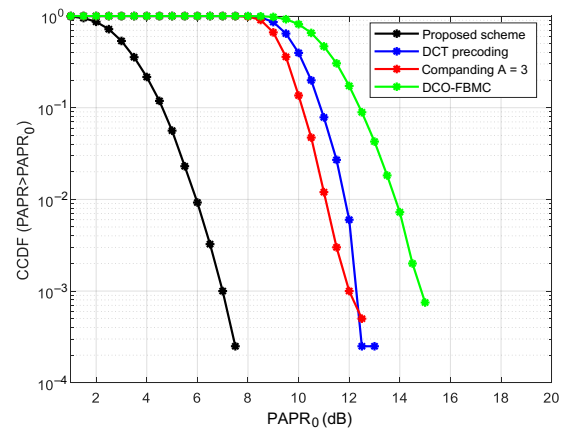


Fig. 7. PAPR CCDF comparison of FBMC-based VLC reduction techniques at  $N=64$ .

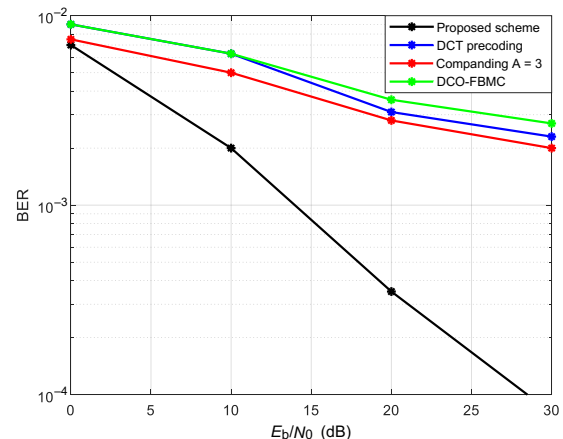


Fig. 8. PAPR CCDF comparison of FBMC-based VLC reduction techniques at  $N=128$ .

Figures 9 and 10 depict the BER performance of the suggested reduction approach with other PAPR reduction schemes. Using the proposed scheme in the FBMC PAPR reduction provides an improved BER performance. When the number of subcarriers  $N = 64$  and  $N = 128$  is considered, the DCT precoding and companding techniques have the same BER as the DCO-FBMC technique, whereas the proposed scheme has lower BER than them and the BER performance is significantly improved, it achieves  $10^{-4}$  BER with  $E_b/N_0 = 30$  dB and 28 dB for  $N = 64$  and  $N = 128$ , respectively.

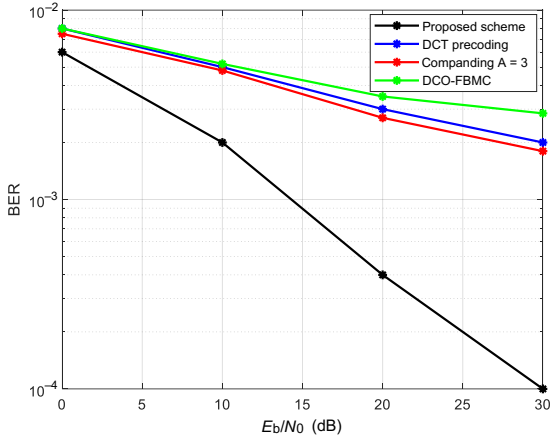


Fig. 9. BER performance comparison of FBMC-based VLC reduction techniques at  $N = 64$ .

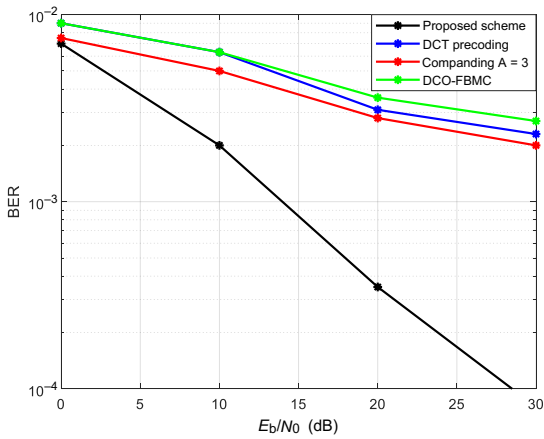


Fig. 10. BER performance comparison of FBMC-based VLC reduction techniques at  $N = 128$ .

The simulated PSD of the proposed scheme vs. DCT precoding, companding, and original DCO-FBMC is illustrated in Fig. 11. It is clear from this figure that using the proposed scheme in FBMC PAPR reduction does not affect the PSD; it remains nearly unchanged compared to PSD of the original DCO-FBMC and other reduction techniques. In other words, the proposed scheme succeeds in improving PAPR and BER performance without increment in the OOB emission.

In the proposed scheme, an alternative technique to DC bias called the addition reversed FBMC was used. It involves dividing the bipolar signal into positive and negative parts, and the negative part is applied to the number of adders denoted by  $I$ . Figure 12 demonstrates the effect of the number of adders  $I$  on PAPR and BER,

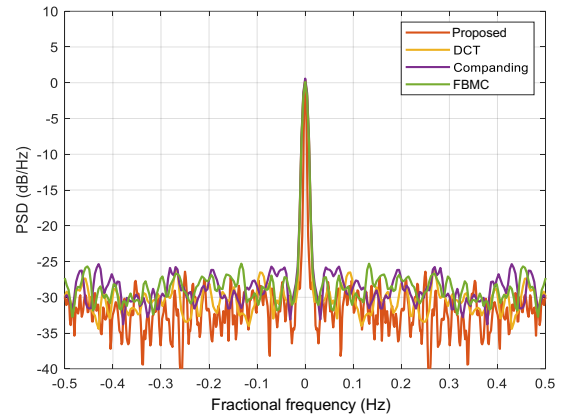


Fig. 11. PSD comparison of FBMC based VLC reduction techniques.

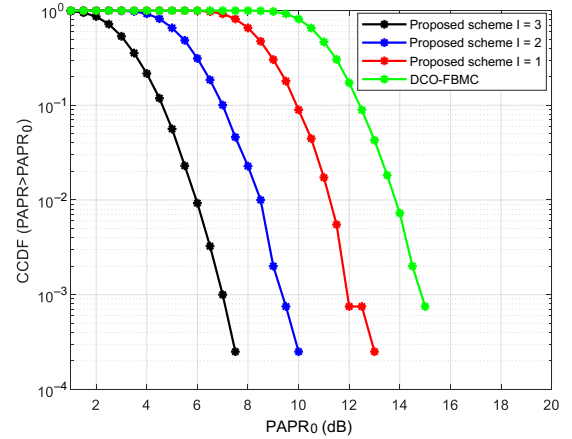


Fig. 12. Number of adders effect on the proposed scheme PAPR's CCDF.

respectively. It is obvious that as the number of  $I$  increases, the PAPR reduction is boosted at the same time BER is not changed. Thus, in the simulation,  $I = 4$  is used.

To evaluate the proposed scheme accurately in terms of its design target, a comparison, is presented in Table 2, between the suggested approach and other approaches in terms of a computational complexity overhead. The computational complexity was measured, based on the real multiplications (RMs) only, since RM includes more computation complexity than real additions (RAs) [34]. In the proposed scheme, there are two candidate visible waveforms based on the DFT cyclic time-shift property. This means that the PPN is processed two times, one for the first candidate signal and another for the second waveform.

Table 2.

Complexity overhead comparison for different FBMC-based VLC reduction techniques.

PAPR reduction technique	Complexity overhead formula/symbol	RMs at $N = 64$
Proposed scheme	$4KN$	1024
DCT precoding	$3N \log_2 N + N$	1216
Companding	$(t + 1)6N, t = 5$	2304

The number of RMs of the PPN is given by  $4KN$  [37]. The addition reversed FBMC has no RMs because the waveform is added to its original form. The RMs number

in the case of companding technique is given by  $(t + 1)6N$ , where  $t$  is the number of terms in Taylor series, which is sufficiently set to 5 [38]. The DCT precoding used in this paper is DCT-2 which has RMs equal to  $3M\log_2N + N$  [39]. The proposed approach maximizes the amount of PAPR reduction better than DCT and companding techniques with lower complexity overhead. Table 2 demonstrates the complexity overhead of the PAPR reduction techniques over the original DCO-FBMC at  $N = 64$ . It is depicted that using the proposed scheme reduces the complexity overhead by 15.7% and 55.55% over DCT and companding techniques, respectively.

## 5. Conclusions

In this research, a PAPR reduction approach for FBMC-based VLC systems is proposed. Its exceptional performance in comparison to other PAPR reduction methods mentioned in the literature in terms of PAPR reduction amount, BER, PSD, and complexity overhead is proved. First, the authors proposed an algorithm based on generating two candidate versions of visible light waveform with different PAPR, by making use of IDFT cyclic time-shift property and selecting only the waveform with smaller peak power to be transmitted over a visible channel. Second, an alternative method to DC bias was proposed, which was named an addition reversed FBMC, for the purpose of enhancing PAPR reduction amount and improving BER performance, as the DC bias limited the PAPR reduction performance of the proposed candidate algorithm. Simulation results demonstrated that compared to other reduction techniques in literature, specifically to DCT precoding and companding techniques, the proposed scheme had a larger PAPR reduction amount, significant improvement in BER, and a larger reduction in complexity overhead without any extra losses in OOB. Consequently, the proposed method significantly enhances many new communication technologies, such as satellite communications, 5G, and hybrid technologies.

## References

- [1] Matheus, L. E. M., Vieira, A. B., Vieira, L. F. M., Vieira, M. A. M., & Gnawali, O. Visible light communication: concepts, applications and challenges. *IEEE Commun. Surv. Tutor.* **21**, 3204–3237 (2019). <https://doi.org/10.1109/comst.2019.2913348>
- [2] Ciaramella, E. *et al.* Prospects of Visible Light Communications in Satellites. in *22nd International Conference on Transparent Optical Networks (ICTON)* 1–4 (2020). <https://doi.org/10.1109/icton51198.2020.9203541>
- [3] Arfaoui, M. A. *et al.* Physical layer security for visible light communication systems: A survey. *IEEE Commun. Surv. Tutor.* **22**, 1887–1908 (2020). <https://doi.org/10.1109/comst.2020.2988615>
- [4] Niarchou, E., Boucouvalas, A. C., Ghassemlooy, Z., Alves, L. N. & Zvanovec, S. Visible Light Communications for 6G Wireless Networks. in *Third South American Colloquium on Visible Light Communications (SACVLC)* 01–06 (2021). <https://doi.org/10.1109/sacvlc53127.2021.9652231>
- [5] Salem, M. A., Tarrad, I. F., Youssef, M. I. & El-Kader, S. M. A. An adaptive EDCA selfishness-aware scheme for dense WLANs in 5G networks. *IEEE Access* **8**, 47034–47046 (2020). <https://doi.org/10.1109/access.2020.2979052>
- [6] Amanor, D. N., Edmonson, W. W. & Afghah, F. Intersatellite communication system based on visible light. *IEEE Trans. Aerosp. Electron. Syst.* **54**, 2888–2899 (2018). <https://doi.org/10.1109/taes.2018.2832938>
- [7] Raeen, M. S., Nella, A. & Rajagopal, M. Design and analysis of a miniaturized UWB plasmonic absorber in visible light spectrum. *Optik* **261**, 169090 (2022). <https://doi.org/10.1016/j.ijleo.2022.169090>
- [8] Shrivastava, S., Agarwal, S. & Chen, B. Asset Allotment in Hybrid RF/VLC Communication in the 400–700 THz Band. in *Terahertz Wireless Communication Components and System Technologies* 211–230 (Springer, 2022). [https://doi.org/10.1007/978-981-16-9182-9\\_14](https://doi.org/10.1007/978-981-16-9182-9_14)
- [9] Aller, D. G., Lamar, D. G., Miaja, P. F., Rodriguez, J. & Sebastian, J. Taking advantage of the sum of the light in outphasing technique for visible light communication transmitter. *IEEE Trans. Emerg. Sel. Topics Power Electron.* **9**, 138–145 (2021). <https://doi.org/10.1109/jestpe.2020.2965774>
- [10] Wang, F., Yang, F., Song, J. & Han, Z. Access frameworks and application scenarios for hybrid VLC and RF systems: state of the art, challenges, and trends. *IEEE Commun. Mag.* **60**, 55–61 (2022). <https://doi.org/10.1109/mcom.001.2100748>
- [11] Rodriguez, J., Lamar, D. G., Miaja, P. F., Aller, D. G. & Sebastian, J. Power-efficient VLC transmitter based on pulse-width modulated DC–DC converters and the split of the power. *IEEE Trans. Power Electron.* **34**, 1726–1743 (2019). <https://doi.org/10.1109/tpel.2018.2830881>
- [12] Hu, J. *et al.* 46.4 Gbps visible light communication system utilizing a compact tricolor laser transmitter. *Opt. Express* **30**, 4365 (2022). <https://doi.org/10.1364/oe.447546>
- [13] El-Ganiny, M. Y., Khalaf, A. A. M., Hussein, A. I. & Hamed, H. F. A. A proposed preamble channel estimation scheme for flip FBMC-based indoor VLC systems. *Opto-Electron. Rev.* **30**, e140859 (2022). <https://doi.org/10.24425/opelre.2022.140859>
- [14] Kumar, S. & Singh, P. Effect of shadowing and background radiation on optical OQAM-FBMC based visible light communication system. *Opt. Quantum Electron.* **54**, 61 (2021). <https://doi.org/10.1007/s11082-021-03437-2>
- [15] Chen, M. *et al.* Precoding-enabled FBMC/OQAM for short-reach IMDD transmission. *IEEE Photon. Technol. Lett.* **33**, 1305–1308 (2021). <https://doi.org/10.1109/lpt.2021.3118838>
- [16] AboulDahab, M. A., Fouad, M. M. & Roshdy, R. A. A Proposed Preamble Based Channel Estimation Method For FBMC in 5G Wireless Channels. in *35th National Radio Science Conference (NRSC)* 140–148 (2018). <https://doi.org/10.1109/nrsc.2018.8354382>
- [17] AboulDahab, M. A., Fouad, M. M. & Roshdy, R. A. Generalized discrete fourier transform for FBMC peak to average power ratio reduction. *IEEE Access* **7**, 81730–81740 (2019). <https://doi.org/10.1109/access.2019.2921447>
- [18] Roshdy, R. A., AboulDahab, M. A. & Fouad, M. M. A modified interference approximation scheme for improving preamble based channel estimation performance in FBMC system. *Int. J. Comput. Netw. Commun.* **12**, 19–35 (2020). <https://doi.org/10.5121/ijcnc.2020.12102>
- [19] Chen, M., Cai, Y., Zhou, J., Zhou, H., Liu, Y. & Chen, Q. Bandwidth enhancement with DAC-enabled pre-equalization and real-valued precoding for a FBMC-VLC. *Opt. Lett.* **47**, 4826 (2022). <https://doi.org/10.1364/ol.472079>
- [20] Salem, M. A., Aboul-Dahab, M. A., Abd El-kader, S.M. & Roshdy, R. A. Performance improvement for the single carrier in FBMC systems by PAPR reduction. *Int. J. Comput. Netw. Commun.* **14**, 17–30 (2022). <https://doi.org/10.5121/ijcnc.2022.14502>
- [21] Chen, R. *et al.* Visible Light Communication Using DC-Biased Optical Filter Bank Multi-Carrier Modulation. in *2018 Global LIFI Congress (GLC)* 1–6 (2018). <https://doi.org/10.23919/glc.2018.8319094>
- [22] Abdalla, H. F., Hassan, E. S. & Dessouky, M. I. Peak to average power ratio (PAPR) reduction in filter bank multicarrier (FBMC) and orthogonal frequency division multicarrier (OFDM) based visible light communication systems. *J. Opt. Commun. Netw.* **2020**, 000010151520200085 (2020). <https://doi.org/10.1515/joc-2020-0085>
- [23] Shi, J., He, J., Zhang, R. & Deng, R. Experimental demonstration of blind equalization for OFDM/OQAM-VLC system. *Opt. Eng.* **58**, 066106 (2019). <https://doi.org/10.1117/1.oe.58.6.066106>
- [24] El-Ganiny, M. Y., Khalaf, A. A. M., Hussein, A. I. & Hamed, H. F. A. Hybrid PAPR reduction schemes for different OFDM-based VLC systems. *Opto-Electron. Rev.* **30**, e141951 (2022). <https://doi.org/10.24425/opelre.2022.141951>

- [25] Valluri, S. P., Kishore, V. & Vakamulla, V. M. A new selective mapping scheme for visible light systems. *IEEE Access* **8**, 18087–18096 (2020). <https://doi.org/10.1109/access.2020.2968344>
- [26] Huang, Y. *et al.* On Improving the Accuracy of Visible Light Positioning System with SLM-Based PAPR Reduction Schemes. in *IEEE International Symposium on Broadband Multimedia Systems and Broadcasting (BMSB)* 1–5 (2020). <https://doi.org/10.1109/bmsb49480.2020.9379574>
- [27] Bera, K., Bakaul, M. & Karmakar, N. A Semi-Deterministic Approach for Clipping Noise Mitigation in DCO-OFDM Systems. in *25th Asia-Pacific Conference on Communications (APCC)* 122–125 (2019). <https://doi.org/10.1109/apcc47188.2019.9026520>
- [28] Gao, Y.-L., Wu, Z.-Y., Wang, Z.-K. & Wang, J. A 1.34-Gb/s real-time Li-Fi transceiver with DFT-spread-based PAPR mitigation. *IEEE Photon. Technol. Lett.* **30**, 1447–1450 (2018). <https://doi.org/10.1109/lpt.2018.2852662>
- [29] Salama, G. M. *et al.* PAPR reduction technique for FBMC based visible light communication systems. *IET Commun.* **16**, 1807–1814 (2022). <https://doi.org/10.1049/cmu2.12430>
- [30] Abdalla, H. F., Hassan, E. S., Dessouky, M. I. & Elsafrawy, A. Three-layer PAPR reduction technique for FBMC based VLC systems. *IEEE Access* **9**, 102908–102916 (2021). <https://doi.org/10.1109/access.2021.3098776>
- [31] Li, Y., Qiu, H., Chen, X. & Fu, J. A novel PAPR reduction algorithm for DCO-OFDM/OQAM system in underwater VLC. *Opt. Commun.* **463**, 125449 (2020). <https://doi.org/10.1016/j.optcom.2020.125449>
- [32] Freag, H., Hassan, E. S., El-Dolil, S. A. & Dessouky, M. I. New hybrid PAPR reduction techniques for OFDM-based visible light communication systems. *J. Opt. Commun. Netw.* **39**, 427–435 (2018). <https://doi.org/10.1515/joc-2017-0002>
- [33] Na, D. & Choi, K. DFT spreading-based low PAPR FBMC with embedded side information. *IEEE Trans. Commun.* **68**, 1731–1745 (2020). <https://doi.org/10.1109/tcomm.2019.2918526>
- [34] Na, D. & Choi, K. Low PAPR FBMC. *IEEE Trans. Wirel. Commun.* **17**, 182–193 (2018). <https://doi.org/10.1109/twc.2017.2764028>
- [35] Qasim, A. A., Mohammedali, H. N., Abdullah, M. F. L., Talib, R. & Dhaam, H. Z. Enhanced Flip-FBMC visible light communication model. *Indones. J. Electr. Eng. Comput. Sci.* **23**, 1783–1793 (2021). <https://doi.org/10.11591/ijeecs.v23.i3.pp1783-1793>
- [36] Li, X. *et al.* A Hybrid TSLM and SA\$-Law Companding Scheme for PAPR Reduction in FBMC-OQAM Systems. in *2020 International Wireless Communications and Mobile Computing (WCMC)* 1077–1081 (2020). <https://doi.org/10.1109/iwcmc48107.2020.9148283>
- [37] Kollar, Z. & Al-Amaireh, H. FBMC transmitters with reduced complexity. *Radioengineering* **27**, 1147–1154 (2018). <https://doi.org/10.13164/re.2018.1147>
- [38] Mounir, M., El\_Mashade, M. B., Berra, S., Gaba, G. S. & Masud, M. A novel hybrid precoding-companding technique for peak-to-average power ratio reduction in 5G and beyond. *Sensors* **21**, 1410 (2021). <https://doi.org/10.3390/s21041410>
- [39] Perera, S. M. & Liu, J. Complexity reduction, self/completely recursive, radix-2 DCT I/IV algorithms *J. Comput. Appl. Math.* **379**, 112936 (2020). <https://doi.org/10.1016/j.cam.2020.112936>